Article

Not peer-reviewed version

Hydrogen Production by Steam Reforming of Ethanol and Dry Reforming of Methane with CO2 on Ni/Vermiculite: Stability Improvement via Acid-Base Treatment of the Support

Hanane Mahir , Abdellah Benzaouak * , Farah Mesrar , Adnane El Hamidi , Mohamed Kacimi , Luca Consentino , Leonarda Francesca LIOTTA *

Posted Date: 1 April 2024

doi: 10.20944/preprints202404.0079.v1

Keywords: Dry reforming, steam reforming, nickel catalyst, vermiculite, clay, mixed oxide

Article

Hydrogen Production by Steam Reforming of Ethanol and Dry Reforming of Methane with CO_2 on Ni/Vermiculite: Stability Improvement via Acid-Base Treatment of the Support

Hanane Mahir [1,2], Abdellah Benzaouak [1,2,*], Farah Mesrar [1], Adnane EL Hamidi [2], Mohamed Kacimi [1], Luca Consentino [3] and Leonarda F. Liotta [3,*]

[1] Laboratory of Nanomaterials, Nanotechnologies and Environment, Physical- Chemistry of Materials, Catalysis and Environment Unity, Department of Chemistry, Faculty of Sciences, Mohammed V University in Rabat, Faculty of Sciences, Avenue Ibn Battouta, BP:1014, 10000 Rabat, Morocco

[2] Laboratory of Spectroscopy, Molecular Modelling, Materials, Nanomaterials, Water and Environment, Environmental Materials Team, ENSAM, Mohammed V University in Rabat, B.P. 6207 Avenue des Forces Armées Royales, Rabat- Morocco

[3] Istituto per lo Studio dei Materiali Nanostrutturati (ISMN)-CNR, via Ugo La Malfa, 153, 90146 Palermo, Italy

* Correspondence: leonardafrancesca.liotta@cnr.it (L.F.L.); abdellah.benzaouak@ensam.um5.ac.ma (A.B.)

Abstract: In this study, vermiculite was explored as a support material for nickel catalysts in two key processes in syngas production through dry reforming of methane with CO_2 and steam reforming of ethanol. The vermiculite was subjected to acid or base treatment, then, Ni catalysts were prepared through incipient wetness impregnation and characterized using various techniques, including X-ray, FTIR, temperature programmed reduction (H_2-TPR). TG-TD analyses were performed to assess the formation of carbon deposits on spent catalysts. The Ni based catalysts were used in the reaction tests without a reduction pre-treatment. Initially, raw vermiculite-supported nickel showed limited catalytic activity, however after acid (Ni/VTA) or base (Ni/VTB) treatment, vermiculite became an effective support for nickel in dry methane reforming. The resulting catalysts (Ni/VTB and Ni/VTA) displayed outstanding performance, with high methane conversion and hydrogen yield. Acidic treatment improved the reduction of nickel species and reduced carbon deposition, outperforming alkali treatment. The prepared catalysts were also explored in ethanol steam reforming. The performance was investigated as a function of the temperature, water/ethanol ratio, and space velocity, with acid-treated catalysts performing as the best. The study emphasized the importance of contact time with the catalyst and addressed challenges related to carbon formation and sintering for long-term stability. In conclusion, acidic treatment of the vermiculite support, before Ni deposition, significantly enhanced the catalytic activity and stability of nickel catalysts in both dry methane reforming and ethanol steam reforming processes.

Keywords: dry reforming; steam reforming; nickel catalyst; vermiculite; clay; mixed oxide

1. Introduction

In recent decades, mining activities have experienced significant growth, driven by advances in technology. Paradoxically, these mining operations have become major generators of waste on a large scale, necessitating efficient waste management strategies. In this context, one avenue for addressing the pollution stemming from these activities and adding value to mining operations is the valorization of this waste as catalysts [1].

The concept of a heterogeneous catalyst for various reactions involves the combination of an active phase deposited on a support. This support provides the catalyst with porosity, mechanical

 doi:10.20944/preprints202404.0079.v1

resilience, and facilitates the even dispersion of the active component [2]. Consequently, the support must possess a high specific surface area, and in some cases, it may play a pivotal role in the reaction mechanism, displaying catalytic activity itself, which is often referred to as bifunctional behavior.

In dry reforming of methane (DRM), the nature of the species involved, the dispersion and size of the metal particles, and their interactions with the support significantly influence the catalystic performances [3]. Alkaline and/or alkaline earth metals, despite lacking direct catalytic activity, often impact the acidity and basicity of the catalyst. Additionally, rare earth oxides help minimize carbon deposition and the sintering of active metals.

Commonly used catalysts feature transition metals (Fe, Co, Ni, Cu) supported on various materials (silica, alumina, and MgO) and exhibit good activity. However, a notable drawback is the deposition of carbonaceous materials, which leads to performance degradation. Catalysts based on noble metals (Pt, Pd, Ru, etc.) demonstrate high selectivity in catalytic methane reforming and are less prone to carbon deposits [3–6]. However, their elevated cost diminishes their economic appeal. Unfortunately, carbon formation, known as coking, typically occurs due to methane decomposition and CO disproportionation, leading to catalyst deactivation or destruction.

Research efforts have primarily concentrated on developing new catalysts that resist carbon formation while maintaining cost-effectiveness and availability compared to traditional nickel catalysts on conventional oxides like SiO_2, Al_2O_3, and $MgAl_2O_4$ [7,8]. Previous studies by some of us have yielded promising results in methane dry reforming using Ni-loaded hydroxyapatite, fluorapatite, and precipitated natural phosphate [9,10].

The ongoing quest for diversifying catalytic material resources for economic and environmental reasons has piqued considerable interest. For instance, the use of natural clay as a support or catalyst has gained attention [11]. Furthermore, solid materials derived from mining residues are rich in components typically employed in catalysis. Utilizing mining materials as catalysts or supports presents a compelling alternative to traditional materials such as silica and alumina, primarily due to their low cost, ready availability, and permeability [11]. Other advantages include ease of shaping and the adaptability to specific application requirements. The potential for chemical modification of clays further enhances their utility across a range of technological applications, thereby adding value to this abundant natural resource [11–13].

In this context, we present the development of a novel catalyst derived from mining residues with negative value. Specifically, we report on the synthesis of a Ni catalyst supported by expanded vermiculite that has undergone acid or base treatment. Vermiculite is an aluminosilicate clay mineral with a layered structure [12–14]. Both in its natural form and when expanded, vermiculite exhibits exceptional characteristics such as lightweightness, durability, and eco-friendliness (it is chemically inert and completely non-toxic). It has found extensive use in heavy metal adsorption [13,14]. While the literature has documented a few applications of vermiculite as a catalyst [14,15] or catalyst support [16,17], its potential remains underexplored.

The primary objective of this study is to evaluate the catalytic performance of nickel-loaded expanded vermiculite subjected to acid or base treatment. This novel substrate is assessed in the processes of carbon dioxide reforming of methane [16–18] and steam reforming of ethanol, particularly under low-temperature conditions. The catalysts are synthesized and comprehensively characterized using various techniques, including X-ray diffraction, FTIR spectroscopy, TG-DT analyses, and temperature-programmed reduction (H_2-TPR). This investigation marks the inaugural phase of a series aimed at scrutinizing specific catalytic systems employed in the realm of hydrogen production.

2. Experimental

2.1.1. Catalyst Preparation

All chemicals employed in this study were of analytical quality (sourced from Aldrich and Fluka) and were employed without additional refinement. The raw expanded vermiculite (VE) employed in this research was provided by Xinjiang Yuli Xinlong Vermiculite Co., Ltd. located in

 doi:10.20944/preprints202404.0079.v1

China. The VE chemical composition is detailed in Table 5-1, mainly composed of 39.78% SiO_2, 22.84% MgO, 20.14% Al_2O_3, 6.12% K_2O, 4.82% Fe_2O_3, 3.14% CaO, 2.12% Na_2O, and 0.87% TiO_2.

The acid-treated vermiculite substrate (VTA) was prepared by leaching the vermiculite with a 1 M hydrochloric acid solution, using a clay mineral mass/hydrochloric acid solution ratio of 1 g/10 cm3. This was carried out at 80°C for 2 hours. The second support, VTB, was obtained by treating VE with NaOH (1 M) at 60°C for 24 hours. VTA and VTB were then washed, filtered and dried at 120°C. They were subsequently calcined at 700°C for 12 hours in an air atmosphere.

The preparation of Ni/VE, Ni/VTA and Ni/VTB catalysts was carried out using the wetness impregnation method, with a Ni loading of 15 wt.%. The impregnated solids were dried at 120°C for 12 hours, then calcined in air at 700°C for 24 hours.

2.1.2. Characterization Methods

The elemental composition of the catalysts was determined using microwave plasma atomic emission spectroscopy (ICP-AES) with an Agilent 4200 spectrometer.

Specific surface area, pore volume and pore size distribution of the samples were measured at −196 ◦C with a nitrogen sorption technique using the ASAP 2020 equipment (Micromeritics, Norcross, Catalysts 2023, 13, 606 15 of 18 GA, USA). Before the measurements, the powder samples (c.a 200 mg) were degassed at 250 ◦C for 2 h. The specific surface area was calculated via the Brunauer-Emmett-Teller (BET) method in the standard pressure range 0.05 – 0.3 P/P_0. The pore volume and pore size distribution were obtained by analysis of the desorption branch, using the Barrett, Joyner and Halenda (BJH) calculation method.

X-ray diffraction patterns were obtained using a Siemens D 5000 high-resolution diffractometer equipped with a copper anticathode ($K\alpha$ = 1.5406 Å). Data were collected over a 2θ range of 5-80° with a scan step of 0.01°. The particles size was calculated using the Scherrer Equation:

$$\boldsymbol{D_{hkl} = \frac{K\lambda}{b\,cos\theta}} \qquad (1)$$

Fourier Transform Infrared (FTIR) spectra were recorded in the range of 400 to 4000 cm^{-1} at room temperature on a Perkin-Elmer 1600 spectrometer using self-supporting KBr disks.

Temperature-programmed reduction (TPR) profiles were recorded at atmospheric pressure using a microreactor containing approximately 100 mg of oxidized catalyst. This technique was selected for studying Ni-loaded vermiculite due to its ability to provide insights into the location of nickel and its interactions with the carrier. Reduction of the samples was carried out using a mixture of H_2/He at a volume ratio of 2.5/60 with a total flow rate of 62.5 cm^3 min and a heating rate of 10 °C min. Hydrogen consumption was monitored using a mass spectrometer.

Thermogravimetric and differential thermal analyses (TGA/DTA) were conducted using a TGA/DSC1 Star System from Mettler Toledo. The evolution of gaseous species was monitored online using a mass quadrupole (Thermostar TM, Balzers).

2.1.3. Catalytic Tests

2.1.1. Methane Reforming Reaction

The methane reforming reaction was investigated in a continuous-flow microreactor made of quartz, maintained at atmospheric pressure. Prior to commencing the reaction, 100 mg of the catalyst were sieved to achieve a grain size ranging from 120 to 180 μm and placed inside the reactor between two quartz wool plugs.

The reaction temperature was ramped up from room temperature to 700°C, utilizing a heating rate of 5°C per minute. A feed mixture consisting of $CH_4/CO_2/N_2$ in a ratio of 2/2/56 was introduced into the reactor, with a total flow rate of 60 ml/min. It is important to note that all catalysts were employed without prior reduction using hydrogen.

Particular emphasis was placed on assessing the stability of the catalysts over the course of the reaction. Hydrocarbons produced during the reaction were analyzed in real-time using an online Delsi chromatograph equipped with a Porapak Q column and a Flame Ionization Detector (FID).

 doi:10.20944/preprints202404.0079.v1

Carbon dioxide and hydrogen concentrations were determined using a second gas chromatograph (Shimadzu, 8A), equipped with a carbosphere column and molecular sieves (5A) columns, coupled with a Thermal Conductivity (TC) detector.

The methane and carbon dioxide conversions and hydrogen yield were calculated as follows:

$$\mathrm{CH_4\ conversion\ (\%)} = \frac{(\mathrm{CH_4})_{\mathrm{in}} - (\mathrm{CH_4})_{\mathrm{out}}}{(\mathrm{CH_4})_{\mathrm{in}}} \mathrm{x100}$$

$$\mathrm{CO_2 conversion\ (\%)} = \frac{(\mathrm{CO_2})_{\mathrm{in}} - (\mathrm{CO_2})_{\mathrm{out}}}{(\mathrm{CO_2})_{\mathrm{out}}} \mathrm{x100}$$

$$\mathrm{H_2\ yield\ (\%)} = \frac{(\mathrm{H_2})_{\mathrm{out}}}{(\mathrm{CH_4})_{\mathrm{in}}} \mathrm{x} \frac{100}{2}$$

$$\mathrm{CO\ yield\ (\%)} = \frac{\mathrm{CO_{out}}}{(\mathrm{CH_4})_{\mathrm{in}} + (\mathrm{CO_2})_{\mathrm{in}}} \mathrm{x100}$$

2.1.2. Ethanol Steam Reforming (ESR)

The catalyst's performance in the ethanol steam reforming (ESR) process was assessed using a quartz tube fixed-bed reactor. Prior to each test, the catalyst underwent in-situ treatment at 700°C in a 1:8 (v/v) H_2:N_2 stream at a flow rate of 60 mL/min for one hour.

Following this pretreatment, the desired water/ethanol ratio was introduced into the evaporator at 150°C using a syringe pump, while an N_2 flow at a rate of 20 ml/min facilitated the vapor transport into the reactor.

The investigation focused on ethanol conversion and gas production. A fresh catalyst was utilized for each test, with a fixed reaction time of 6 hours. The gaseous products obtained at the reactor outlet were analyzed online using gas chromatography (GC) Perichrom PR2100 instrument controlled by Winilab software.

For reactants and products analysis, two detectors were employed: a thermal conductivity detector (TCD) equipped with a TDX-01 column to measure concentrations of H_2, CO_2, and CO. A flame ionization detector (FID) equipped with a Porapak-Q column was utilized to identify potential organic species, including CH_4, C_2H_4, C_2H_6, CH_3CHO, and CH_3COCH_3. Unreacted ethanol was examined offline via FID. The key performance parameters, including ethanol conversion (X_{EtOH}), hydrogen yield (Y_{H2}), and the distribution of gaseous carbon-containing products (CH_4, CO, CO_2, C_2H_4, C_2H_6, CH_3CHO, and CH_3COCH_3), were determined as follows:

$$X_{EtOH}(\%) = \frac{EtOH_{in} - EtOH_{out}}{(EtOH_{out})x100}$$

$$Y_{EtOH}(\%) = \frac{moles\ H_2\ produced}{(6x\ moles\ EtOH\ converted)} x100$$

$$Si(\%) = \frac{mole\ of\ gaseous\ product\ i}{(mole\ all\ gaseous\ products)} x100$$

3. Results and Discussion

3.1. Characterization

3.1.1. X-ray Diffraction

The X-ray diffraction patterns of the supports and the obtained catalysts are presented in Figure 1. The initially expanded vermiculite (VE) (Figure 1A) displayed distinctive diffraction peaks at 2theta angles of 6.24°, 7.45°, and 8.85° (see Figure 1B), indicating the presence of various layers of cations (Mg^{2+}, Ca^{2+}, Na^{+}) within the vermiculite structure. Specifically, the 6.24° peak is characteristic of magnesium in hydrated forms of vermiculite [17], the 12.4 Å spacing could be attributed to partially dehydrated magnesium interlayer cations [18], and the 8.85 Å spacing is related to interlayer

 doi:10.20944/preprints202404.0079.v1

potassium ions [17]. These observations highlight the diversity of cations present in different layers of the vermiculite structure.

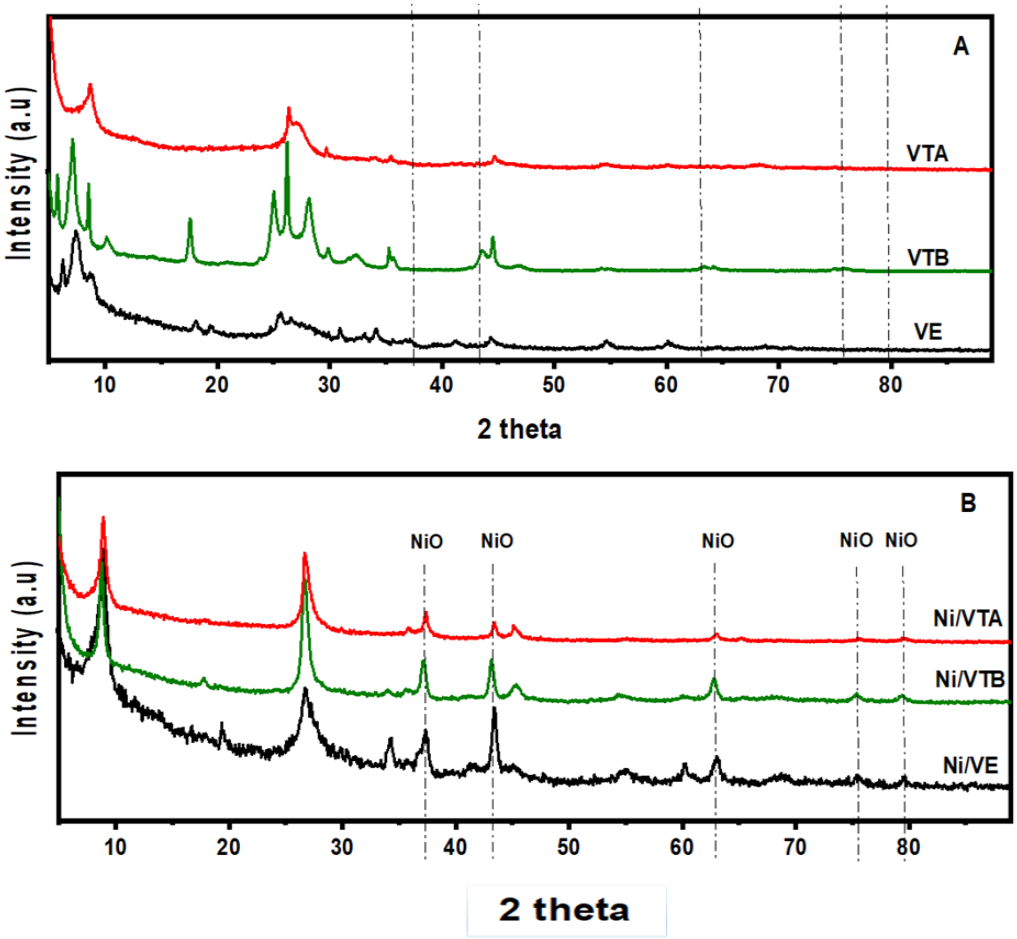

Figure 1. XRD diffractograms of supports (A) and calcined catalysts (B).

Additionally, the peak observed at approximately 2θ = 25.6° can be attributed to the presence of quartz impurities in the vermiculite [19].

The XRD pattern of vermiculite treated with 1 M HCl (VTA) revealed significant changes compared to raw vermiculite (VE). Notably, only one peak at around 8.69° (10.24 Å) with low intensity was observed in VTA. This is characteristic of the protonic form of clay. Consequently, the substitution of interlayer Mg^{2+} and K^{+} cations by hydronium ions during acid treatment resulted in a reduction of the interlayer distance in vermiculite [19]. In the high 2θ range, some reflections remained visible, indicating that a portion of the vermiculite resisted to acid attack. This observation aligns with the chemical analysis presented in Table 1, which indicates that some of the interlayer potassium and magnesium ions were not exchanged during this process.

Furthermore, XRD patterns of vermiculite treated with NaOH solution (VTB) displayed an increase in the intensity of characteristic peaks across the entire 2θ range compared to the starting material. This finding supports the notion that the alkali treatment at 60°C did not significantly affect the clay structure. Table 1 provides additional evidence in this regard.

The chemical analysis revealed that the composition of the material treated with NaOH (VTB) remained unchanged compared to the starting material. This suggests that there was no leaching of the oxide components but rather their in-situ deposition-precipitation [20]. In contrast, acid treatment of vermiculite significantly modified its chemical composition with removal of almost Mg, Al, Fe, K, Ca, Na and Ti oxides, with silica being predominant, at the same time the surface area increased from 36 to 270 m^2/g, together with an increased pore volume moving from Ni/VE to the Ni/VTA catalyst. Conversely, no significant changes were noticed for the surface area and pore volume of Ni catalyst

 doi:10.20944/preprints202404.0079.v1

supported over the material treated with the NaOH solution (Table 1). Both samples, Ni/VE and Ni/VTB showed a broad pore size distribution in the range between 5-30 nm, only the Ni/VTA catalyst according to the increased silica oxide component showed a defined pore size distribution centered at 15 nm.

Table 1. Specific surface area, pore volume and chemical composition of Ni over the raw and treated vermiculite.

Catalysts	SSA ($m^2\ g^{-1}$)	Pore volume ($cm^3\ g^{-1}$)	Chemical composition mass (%) by ICP analysis								
			Ni	SiO_2	MgO	Al_2O_3	Fe_2O_3	K_2O	CaO	Na_2O	TiO_2
Ni/VE	36	0.10	15.0	33.8	19.8	17.1	2.8	5.1	3.2	2.1	1.1
Ni/VTB	38	0.11	15.0	36.4	18.6	16.6	2.6	4.9	2.9	2.0	1.0
Ni/VTA	270	0.55	15.0	78.4	2.8	2.6	0.3	0.5	0.2	0.1	0.1

The X-ray diffraction (XRD) patterns of Ni-supported treated and untreated vermiculite (Figure 1B) displayed characteristic peaks of cubic NiO at $2\theta \approx 37.34$, 43.25, 62.82, 75.56, and 79.65°. Additionally, a new broad peak at 26.8°, attributed to the presence of amorphous silica, was detected in all obtained catalysts [21]. We estimated nanocrystallite sizes using the Debye–Scherrer equation. The average crystallite size of NiO for Ni/VTB and Ni/VTA was found to be 18.3 nm and 17.1 nm, respectively, less than to that of Ni/VE (21 nm).

3.1.2. FTIR Spectroscopy

The FTIR spectra of expanded vermiculite and the prepared catalysts are presented in Figure 2, highlighting the following characteristic bands:

-A band located at 3450 cm^{-1}, attributed to OH stretching (νOH), which signifies hydrogen bonding between SiO-H groups at the surface.

-Another band at 1648 cm^{-1}, associated with the δOH bending vibration of H_2O molecules retained within the silica or alumina.

-Bands at 1000 and 1080 cm^{-1} attributed to the νSi-O asymmetric stretching vibration of SiO_4 and in-plane bending. A band at 668 cm^{-1}, attributed to deformation bands of Si-O. A band at 454 cm^{-1}, related to T-O-T bending vibrations (T=Si or Al). Finally, a band at 724.8 cm^{-1}, attributed to tetrahedral Al-O.

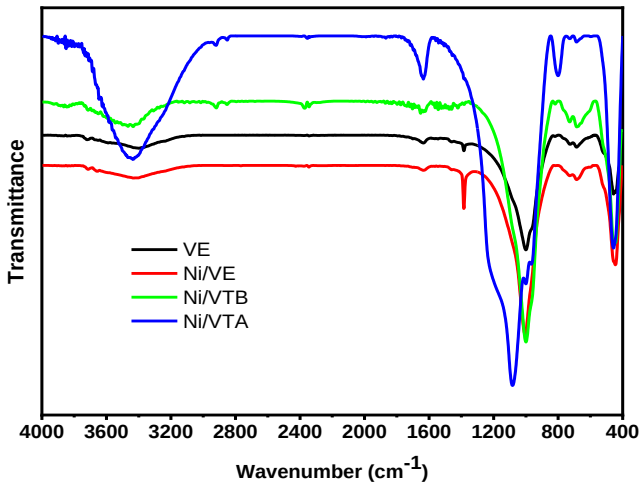

Figure 2. FTIR spectra of VE, Ni/VE, Ni/VTB and Ni/VTA.

 doi:10.20944/preprints202404.0079.v1

The spectra of Ni/VTA reveal a new peak at 795 cm^{-1}, corresponding to the bending vibrations of SiO4 tetrahedra, similar to that observed for amorphous silica in the X-ray diffraction patterns. Notably, the addition of nickel to the supports does not appear to modify the IR spectra.

3.1.3. TPR Analyses

To investigate the reducibility of the Ni/VE, Ni/VTB, and Ni/VTA catalysts, as well as the interaction between the metal species and the support, we conducted Temperature Programmed Reduction (TPR) analyses (Figure 3). Notably, for all the calcined catalysts, the reduction process initiated at relatively low temperatures, near 270°C.

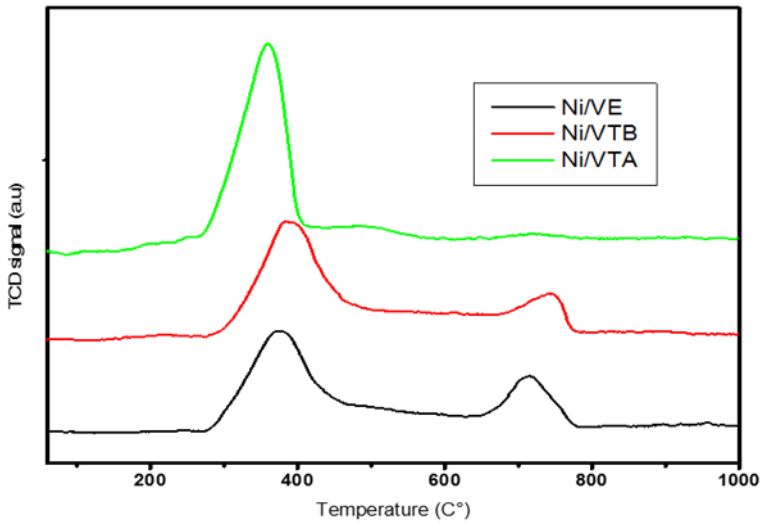

Figure 3. H_2-TPR curves for different catalysts Ni/VE, Ni/VTB and Ni/VTA.

Notably, for all the calcined catalysts, the reduction process initiated at relatively low temperatures, near 270°C.

In the TPR profiles of Ni-supported expanded vermiculite and base-treated vermiculite, two distinct peaks were observed. The primary peak, centered around 370°C, was accompanied by a secondary, weaker hydrogen uptake at higher temperatures, approximately 720°C and 737°C, respectively. This secondary peak can be attributed to the reduction of NiOx species that exhibit strong interactions with the support [22]. In contrast, for Ni-supported vermiculite treated with HCl solution, TPR profiles displayed only a single, main peak around 370°C. This peak was assigned to the reduction of free NiO particles to NiO, which are dispersed over the support [23]. This observation suggests that the Ni species in the acid-treated vermiculite-supported Ni catalysts are more easily reducible. Furthermore, the TPR profiles of Ni/VTA closely resembled those observed for Ni/SiO2, as reported by Y.H. Taufiq-Yap et al. [24].

3.2. Catalytic Activity

3.2.1. Dry Reforming of Methane

It should be noted that in most published studies, nickel-based catalysts undergo a hydrogen pretreatment to determine their activity. In our study, we assessed the catalytic properties for the CO_2 reforming of methane and investigated the impact of alkali and acid activation of vermiculite on the supports. Importantly, the catalysts were utilized without prior reduction. The active phase of the catalysts, NiO_x, was reduced "in situ" during the reaction with a mixture of CH_4 and CO_2, a methodology consistent with other studies [10,23,24]. This approach seeks to develop an active and resilient catalyst that can be employed directly in dry reforming reactions without the need for pre-reduction using H_2, promoting process efficiency on an industrial scale.

 doi:10.20944/preprints202404.0079.v1

For the dry reforming of methane by CO_2 at low temperatures, Ni-based catalysts were tested using expanded vermiculite as a support, as well as vermiculite treated with HCl or NaOH solutions (Figures 4–6). Figure 4 illustrates the evolution of methane conversion as a function of temperature for all the catalysts. Notably, none of the catalysts displayed activity below 520°C.

The activation of methane commenced at approximately 520°C, 560°C, and 580°C for Ni/VTA, Ni/VTB, and Ni/VE, respectively. This activation increased with the reaction temperature, achieving 93% CH_4 conversion at 700°C, compared to 89% and 72% for Ni/VTB and Ni/VE, respectively. This phenomenon is intimately related to the endothermic character of the reaction [25]. Notably, the type of activation treatment did not exert a significant influence on the catalytic activity of the catalysts concerning temperature. However, there was a substantial difference in catalytic activity between raw expanded vermiculite and vermiculite treated with acid or base.

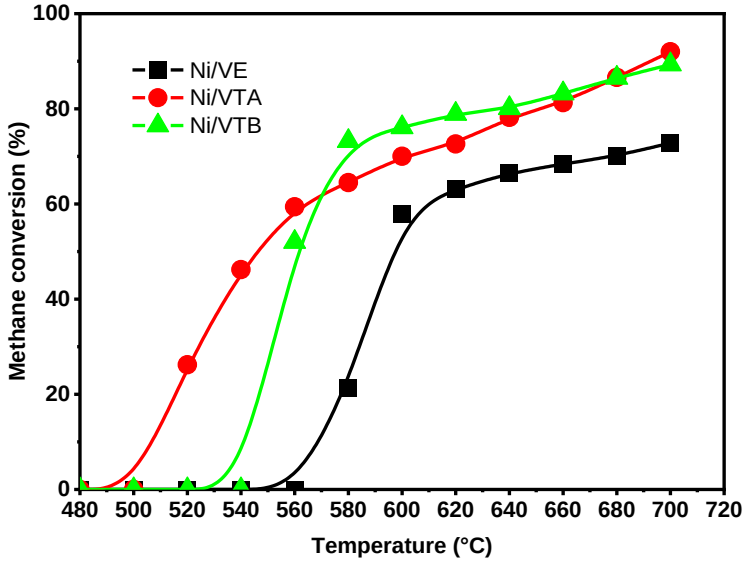

Figure 4. CH_4 conversion over the catalysts Ni/VE, Ni/VTB and Ni/VTA vs the reaction temperature.

The stability of the catalysts under reaction conditions is a critical parameter. Figures 5 and depict CH_4 conversion and H_2 yield versus time on stream, respectively, recorded at 600 °C over Ni/VTA, Ni/VTB, and Ni/VE for 240 minutes. Ni-supported expanded raw vermiculite exhibited poor catalytic activity, undergoing rapid deactivation in CO_2 reforming with methane. Specifically, over Ni/VE, the CH_4 conversion and H_2 yield were decreased, after only 100 minutes on stream, from 60% to 16% and from 49% to 10%, respectively.

In contrast, for Ni-supported base- or acid-treated vermiculite, the results in Figures 5 and 6 revealed that CH_4 conversion only decreased from 76% to 61%, and hydrogen yield slightly decreased from 65% to 57% over the Ni/VTB catalyst. Meanwhile, for Ni/VTA, the conversions of CH_4 and H_2 yield slightly changed, from 72% to 67% and from 62% to 58%, respectively, after 240 hours on stream. For all the catalysts, catalytic activity gradually decreased as the duration of the tests increased. However, for Ni/VTA and Ni/VTB, CH_4 conversion decreased by only 5% and 15%, respectively, during 240 minutes on stream. This indicates that acid treatment significantly enhanced the catalytic activity of the catalyst, which is correlated to its easy reducibility at low temperatures.

To determine the type and quantity of carbon deposited on Ni/VTA and Ni/VTB catalysts after 240 minutes of reaction at 600°C, we conducted Thermogravimetric Analysis (TGA-TDA) under air, ranging from room temperature to 800°C (Figure 6A,B). Carbon deposition occurs primarily due to the reactions of CH_4 decomposition (Equation (2)) and CO disproportionation (Equation (3)), which are favorable conditions in CH_4/CO_2 reforming. It's worth noting that the TGA profile of Ni-supported expanded vermiculite shows no mass loss, which aligns with the catalyst's low activity.

 doi:10.20944/preprints202404.0079.v1

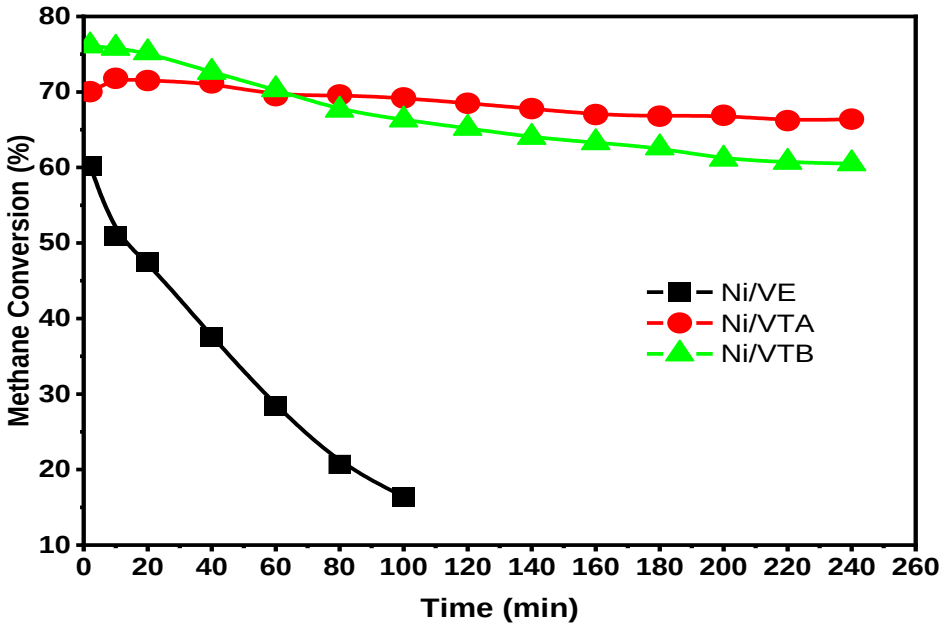

Figure 5. CH_4 conversion over the catalysts Ni/VE, Ni/VTB and Ni/VTA vs. time reaction.

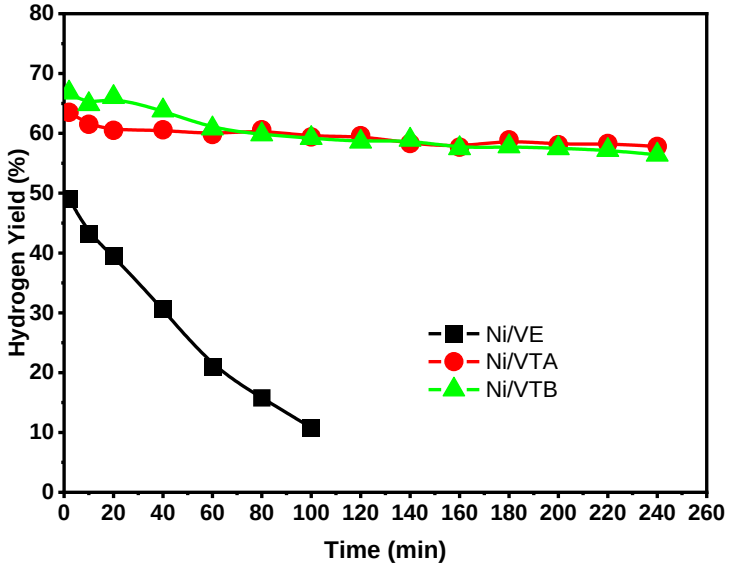

Figure 6. H_2 yield over the catalysts Ni/VE, Ni/VTB and Ni/VTA vs. time reaction.

The TGA results (Figure 6A) revealed that the spent catalysts Ni/VTA and Ni/VTB exhibited an average mass loss across the entire investigated temperature range (30–800°C). The initial weight loss of 4.3% and 1.5% w/w for VTA and VTB, respectively, above 200°C can be attributed to water removal. The weight loss occurring at temperatures below 300°C is related to thermal desorption of water and the removal of easily oxidized carbon species, as reported in previous studies [26–28]. The weight loss observed in the temperature range of 500-650°C is due to coke gasification through the oxidation of coke to CO and CO_2.

 doi:10.20944/preprints202404.0079.v1

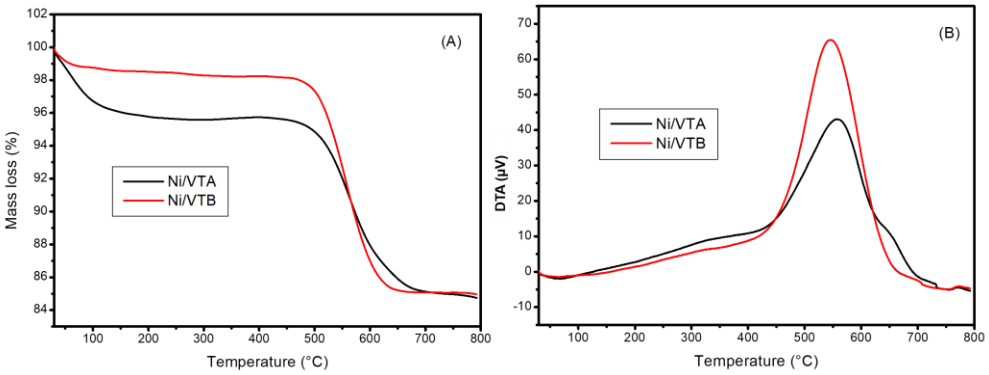

Figure 7. TGA profiles (A) and DTA profiles (B) of spent catalysts, Ni/VTA and Ni/VTB.

Interestingly, the amount of deposited carbon on Ni/VTA (10.5%) is lower than that on Ni/VTB catalyst (13.1%). This trend in carbon deposition parallels the catalytic stability of the catalysts.

The DTA profiles in Figure 6B reveal the presence of a single strong exothermic peak ranging from 450 to 700 °C for both catalysts. The maximum peak temperatures observed for the Ni/VTA and Ni/VTB catalysts were 557°C and 548°C, respectively. This suggests the existence of a specific type of carbon, which can be attributed to the oxidation of filamentous carbon or filament (nanotube de carbone), as previously reported by S. Damyanova et al.[29] and W.D. Zhang [30].

3.2.2. Ethanol Steam Reforming

The Figure 8 illustrates the evolution of ethanol conversion using three nickel-based catalysts supported on vermiculite samples. These samples were obtained by the same preparation above used through different treatments of expanded vermiculite, namely neutral, acidic, or basic treatments. In all cases, the supports were impregnated with Ni nitrates to create 15% Ni catalysts.

It has been observed that the ethanol conversions are significant at the start of the reaction. However, there are notable differences in the behavior of the catalysts based on the type of vermiculite support used.

Catalysts prepared by acid-base treatments exhibited stable activity, with only slight deactivation compared to that prepared using the support from the basic treatment [31]. In contrast, the catalyst produced from untreated vermiculite displayed a different pattern. It started with similar activity of the other catalysts, furthermore, rapidly deactivated after 5 hours of functioning.

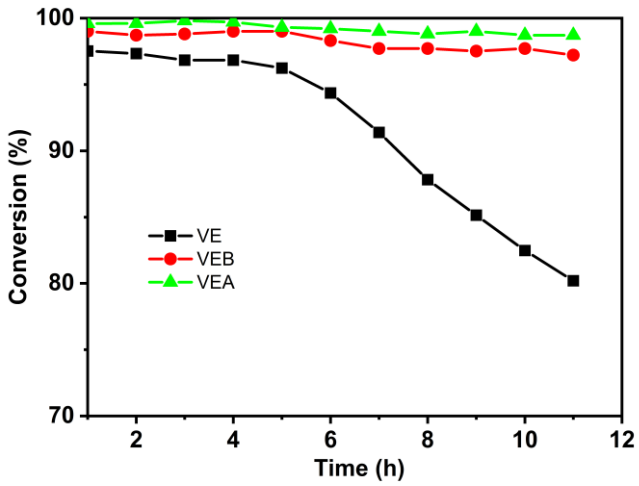

Figure 8. Ethanol conversion vs time over VE, VEA and VEB samples.

 doi:10.20944/preprints202404.0079.v1

To further assess the stability of the prepared catalysts, some experiments were conducted in ESR for a period of 10 hours at 600°C, using a W/F of 18 gcat. The ethanol conversion achieved using the three catalysts is noteworthy, with conversion rates ranging from approximately 98% to 100% after just one hour of reaction. Importantly, this high level of conversion remains relatively stable during the initial five hours of operation. However, it is worth noting that a distinct trend is observed with the 15%Ni/VE catalyst. Initially, it exhibited an impressive ethanol conversion rate of 96.2% at the 5 hour of work time. Nevertheless, beyond this point, there is a gradual decline in its performance, which indicates catalyst deactivation. As is commonly reported in reforming reactions, catalyst deactivation typically stems from two primary factors: carbon formation and sintering on the catalyst [32–35].

In summary, the results highlight the impressive initial performance of the catalysts in achieving high ethanol conversion, with particular attention drawn to the 15%Ni/VE catalyst early success and its later deactivation. However, the observed catalyst deactivation after 5 hours underscores the importance of further investigating and mitigating issues related to carbon formation and sintering for long-term catalyst stability and efficiency. However, one should not overlook the sintering effects initiated by the presence of various cations that are eliminated through acid-base washing [36].

Considering the instability observed in the 15% Ni/VE sample, this study proceeds with the samples obtained from acid-base pre-treated vermiculite. Figure 9A,B illustrate the influence of temperature on the evolution of various reaction products.

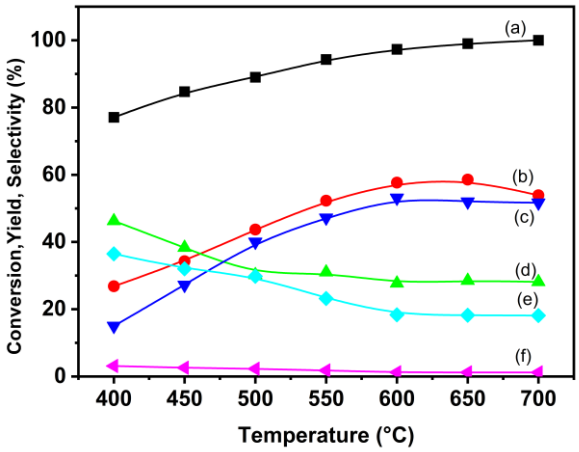

(**A**)

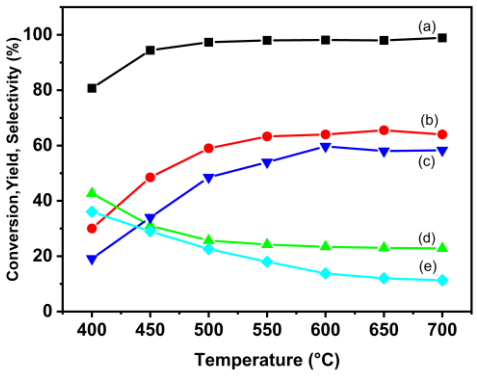

(**B**)

Figure 9. A. (a)Ethanol conversion, (b)Hydrogen Yield, (c)CO_2, (d)CO, (e)CH_4 and (f)C_2H_6 selectivities, over the catalyst: Ni/VTB. **B.** (a)Ethanol conversion, (b)Hydrogen Yield, (c)CO_2, (d)CO, and (e)CH_4 selectivities over the catalyst: Ni/VTA.

 doi:10.20944/preprints202404.0079.v1

The catalytic activity of both catalysts exhibits a noteworthy correlation with the elevation of reaction temperature. For the Ni/VTA catalyst, ethanol conversion approaches near completion at 500°C (Figure 9B), whereas the highest ethanol conversion rate for the Ni/VTB catalyst is achieved at 700°C. At lower temperatures, specifically 400°C, the formation of products such as ethane, ethylene, and acetaldehyde (C2) is observed. This is attributed to the relatively weak C−C bond-breaking ability in the presence of nickel [37–39]. The emergence of acetaldehyde can be attributed to the dehydrogenation of ethanol [40]. Moreover, acetaldehyde is recognized as an intermediate product in ethanol reforming, capable of either decomposing into CO and CH4 through C−C bond cleavage or transforming into ethane and water through C−O cleavage [41].

Figure 10 presents the ethanol conversion data over Ni/VTB (A) and Ni/VTA (B) as a function of the Water/Ethanol ratio. In the case of the two catalysts under examination, 15%Ni/VTB (Figure 10A) and 15% Ni/VTA (Figure 10B), the ethane conversion rate displays an increase as the S/E molar ratio rises, reaching a plateau at a ratio of 9.

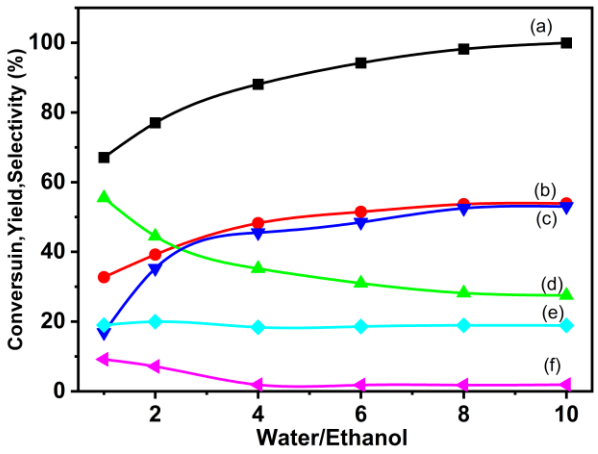

(**A**)

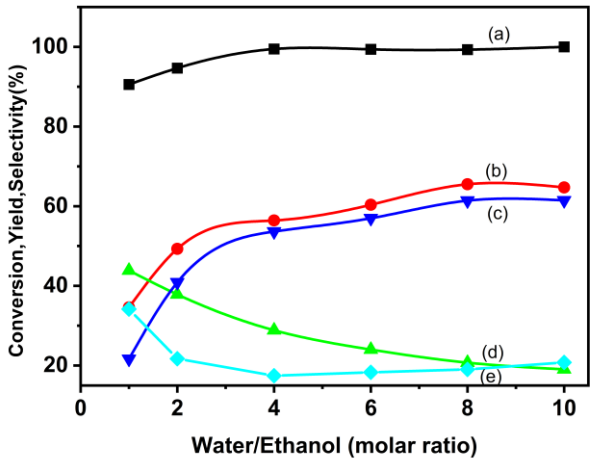

(**B**)

Figure 10. A. (a)Ethanol conversion, (b)Hydrogen Yield, (c)CO_2, (d)CO, (e)CH_4 and (f)C_2H_6 selectivities over the catalyst: Ni/VTB. **B.** (a)Ethanol conversion, (b)Hydrogen Yield, (c)CO_2, (d)CO, (e)CH_4 selectivities over the catalyst: Ni/VTA.

Additionally, there is a simultaneous increase in H2 yield and selectivity for CO_2, while selectivity for CO and CH_4 experience a gradual decline. The presence of an adequate amount of water is associated with an elevation in both ethanol conversion rate and H_2 yield. This outcome is

 doi:10.20944/preprints202404.0079.v1

attributed to the well-established notion that the presence of water generally promotes reforming reactions [42].

Furthermore, upon comparing the performance of the two catalysts, it becomes evident that the catalyst supported by vermiculite and treated with an acid solution outperforms the other. It is essential to highlight that this treatment results in the removal of a portion of the ions situated within the interlayer space. This variance in performance between the two catalysts may be attributed to the differing ease of reduction between them. Notably, in terms of hydrogen production, the acidic catalyst demonstrates a relatively superior performance.

In reactions similar to the reforming process, the study of spatial velocity assumes paramount importance when assessing catalysts from an industrial perspective. The influence of space velocity (W/F) on ethanol conversion rate and product distribution was investigated across a range of spatial velocities, spanning from 12 to 36 gcat·h/mol [EtOH], at a constant temperature of 600°C, while maintaining a molar W/E ratio of 10. As illustrated in Figure 11, the ethanol conversion rate for both studied catalysts exhibited an upward trend with increasing space velocity.

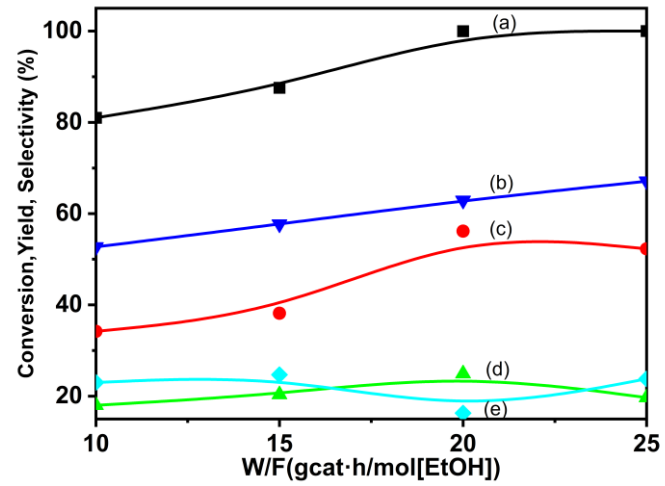

(**A**)

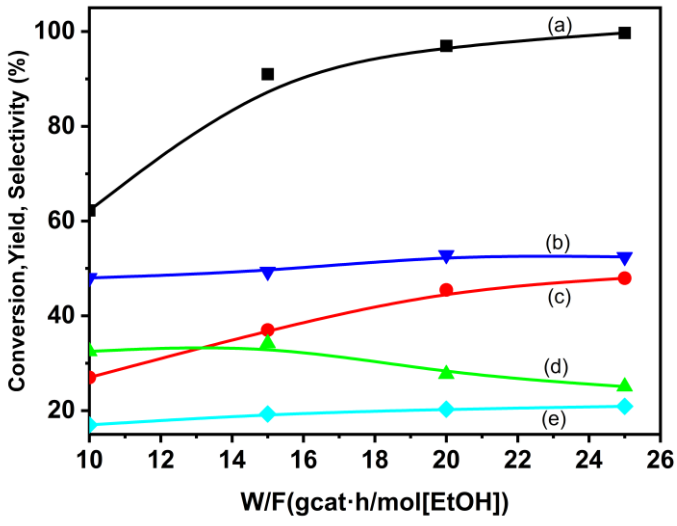

(**B**)

Figure 11. A. (a)Ethanol conversion, (b)Hydrogen Yield, (c)CO_2, (d)CO, (e)CH_4 and (f)C_2H_6 selectivities over the catalyst: Ni/VTB. **B.** (a)Ethanol conversion, (b)Hydrogen Yield, (c)CO_2, (d)CO, (e)CH_4 selectivities over the catalyst: Ni/VTA.

 doi:10.20944/preprints202404.0079.v1

Moreover, there was a corresponding increase in hydrogen yield with the rise in space-time velocity. This phenomenon can be elucidated by considering the contact time between the reactants and the active sites of the catalyst. At shorter space-times, the duration of contact

between the reactants and the active sites becomes too brief, resulting in both low ethanol conversion rates and low hydrogen yields. Conversely, with longer space-times, ethanol molecules enjoy ample contact time with the catalyst, enabling the breaking of C-C and O-H bonds, leading to high ethanol conversion rates and hydrogen yield. It is important to note, however, that as the space-time was increased (ranging from 18 to 36 gcat·h/mol [EtOH]), the ethanol conversion rate and product selectivity exhibited no significant changes.

4. Conclusions

In conclusion, this study investigated the use of vermiculite pure and modified as a support material for nickel catalysts in the processes of hydrogen production through dry reforming of methane with CO_2 and steam reforming of ethanol. The main outcomes and conclusions of this study can be summarized as follows:

The research investigated the impact of acid (Ni/VTA) and base (Ni/VTB) treatments on dry methane reforming and ethanol steam reforming.

Acid-treated catalysts demonstrated superior performance in both processes, showing high methane conversion and hydrogen yield. They also outperformed alkali-treated catalysts in reducing nickel species and minimizing carbon deposition.

Support treatment with vermiculite significantly enhanced catalyst stability and activity. The study highlighted the importance of contact time with the catalyst and addressed challenges related to carbon formation and sintering for long-term stability.

The use of vermiculite as a catalyst support offers a sustainable waste valorization approach. The supported catalysts exhibited high ethanol conversion rates, with stable activity over time. Water presence influenced ethanol conversion rate, hydrogen yield, and selectivity.

Author Contributions: Conceptualization: H.M.; F.M.; A.E.H.; M.K. L.C., A.B.; L.F.L; validation: A.B.; L.F.L; Formal analysis, H.M.; F.M; L.C. writing—original draft preparation, H.M.; F.M.; A.E.H.; M.K. L.C., A.B; writing—review and editing, M.K.; A.B. and L.F.L.; supervision: M.K.; A.B. and L.F.L; All authors have read and agreed to the published version of the manuscript.

Funding: This research was in part funded by Programma di ricerca PE00000021 "NEST—Network 4 Energy Sustainable Transition" CUP: B53C22004060006" and by the European Union – NextGenera on EU from the Italian Ministry of Environment and Energy Security POR H2 AdP MMES/ENEA with involvement of CNR and RSE, PNRR - Mission 2, Component 2, Investment 3.5 "Ricerca e sviluppo sull'idrogeno", CUP: B93C22000630006.

Conflicts of Interest: The authors declare no conflict of interest.

References

1. Vermeiren, W.J.M.; Blomsma, E.; Jacobs, P.A. Catalytic and thermodynamic approach of the oxyreforming reaction of methane. *Catalysis Today* **1992**, *13*, 427-436, doi:https://doi.org/10.1016/0920-5861(92)80168-M.
2. Corthals, S.; Van Nederkassel, J.; Geboers, J.; De Winne, H.; Van Noyen, J.; Moens, B.; Sels, B.; Jacobs, P. Influence of composition of MgAl2O4 supported NiCeO2ZrO2 catalysts on coke formation and catalyst stability for dry reforming of methane. *Catalysis Today* **2008**, *138*, 28-32, doi:https://doi.org/10.1016/j.cattod.2008.04.038.
3. Barroso-Quiroga, M.M.; Castro-Luna, A.E. Catalytic activity and effect of modifiers on Ni-based catalysts for the dry reforming of methane. *International Journal of Hydrogen Energy* **2010**, *35*, 6052-6056, doi:https://doi.org/10.1016/j.ijhydene.2009.12.073.
4. Asami, K.; Li, X.; Fujimoto, K.; Koyama, Y.; Sakurama, A.; Kometani, N.; Yonezawa, Y. CO2 reforming of CH4 over ceria-supported metal catalysts. *Catalysis Today* **2003**, *84*, 27-31, doi:https://doi.org/10.1016/S0920-5861(03)00297-9.
5. Bradford, M.C.J.; Vannice, M.A. CO2 Reforming of CH4. *Catalysis Reviews* **1999**, *41*, 1-42, doi:10.1081/CR-100101948.

6. Rostrupnielsen, J.R.; Hansen, J.H.B. CO2-Reforming of Methane over Transition Metals. *Journal of Catalysis* **1993**, *144*, 38-49, doi:https://doi.org/10.1006/jcat.1993.1312.
7. Selvarajah, K.; Phuc, N.H.H.; Abdullah, B.; Alenazey, F.; Vo, D.-V.N. Syngas production from methane dry reforming over Ni/Al2O3 catalyst. *Research on Chemical Intermediates* **2016**, *42*, 269-288, doi:10.1007/s11164-015-2395-5.
8. Juan-Juan, J.; Román-Martínez, M.C.; Illán-Gómez, M.J. Nickel catalyst activation in the carbon dioxide reforming of methane: Effect of pretreatments. *Applied Catalysis A: General* **2009**, *355*, 27-32, doi:https://doi.org/10.1016/j.apcata.2008.10.058.
9. Boukha, Z.; Kacimi, M.; Pereira, M.F.R.; Faria, J.L.; Figueiredo, J.L.; Ziyad, M. Methane dry reforming on Ni loaded hydroxyapatite and fluoroapatite. *Applied Catalysis A: General* **2007**, *317*, 299-309, doi:https://doi.org/10.1016/j.apcata.2006.10.029.
10. Mesrar, F.; Kacimi, M.; Liotta, L.F.; Puleo, F.; Ziyad, M. Hydrogen production on Ni loaded apatite-like oxide synthesized by dissolution-precipitation of natural phosphate. *International Journal of Hydrogen Energy* **2017**, *42*, 19458-19466, doi:https://doi.org/10.1016/j.ijhydene.2017.04.286.
11. Zhang, J.; Liu, T.; Chen, R.; Liu, X. Vermiculite as a natural silicate crystal for hydrogen generation from photocatalytic splitting of water under visible light. *RSC Advances* **2014**, *4*, 406-408, doi:10.1039/C3RA45301D.
12. Gharin Nashtifan, S.; Azadmehr, A.; Maghsoudi, A. Comparative and competitive adsorptive removal of Ni2+ and Cu2+ from aqueous solution using iron oxide-vermiculite composite. *Applied Clay Science* **2017**, *140*, 38-49, doi:https://doi.org/10.1016/j.clay.2016.12.020.
13. Liu, Y.; Li, H.; Zhu, X.-H. Competitive Adsorption of Ag+, Pb2+, Ni2+, and Cd2+ Ions on Vermiculite. *Separation Science and Technology* **2010**, *45*, 277-287, doi:10.1080/01496390903255572.
14. Chmielarz, L.; Rutkowska, M.; Jabłońska, M.; Węgrzyn, A.; Kowalczyk, A.; Boroń, P.; Piwowarska, Z.; Matusiewicz, A. Acid-treated vermiculites as effective catalysts of high-temperature N2O decomposition. *Applied Clay Science* **2014**, *101*, 237-245, doi:https://doi.org/10.1016/j.clay.2014.08.006.
15. Chmielarz, L.; Wojciechowska, M.; Rutkowska, M.; Adamski, A.; Węgrzyn, A.; Kowalczyk, A.; Dudek, B.; Boroń, P.; Michalik, M.; Matusiewicz, A. Acid-activated vermiculites as catalysts of the DeNOx process. *Catalysis Today* **2012**, *191*, 25-31, doi:https://doi.org/10.1016/j.cattod.2012.03.042.
16. Xin, H.; Yu, F.; Zhu, M.-Y.; Ouyang, F.-H.; Dai, B.; Dan, J.-M. Hydrochlorination of acetylene using expanded multilayered vermiculite (EML-VMT)-supported catalysts. *Chinese Chemical Letters* **2015**, *26*, 1101-1104, doi:https://doi.org/10.1016/j.cclet.2015.05.020.
17. Marcos, C.; Arango, Y.C.; Rodriguez, I. X-ray diffraction studies of the thermal behaviour of commercial vermiculites. *Applied Clay Science* **2009**, *42*, 368-378, doi:https://doi.org/10.1016/j.clay.2008.03.004.
18. Węgrzyn, A.; Chmielarz, L.; Zjeżdżałka, P.; Jabłońska, M.; Kowalczyk, A.; Żelazny, A.; Vázquez Sulleiro, M.; Michalik, M. Vermiculite-based catalysts for oxidation of organic pollutants in water and wastewater. *Acta Geodynamica et Geomaterialia* **2013**, *10*, 341-352, doi:10.13168/AGG.2013.0033.
19. Maqueda, C.; Perez-Rodriguez, J.L.; Šubrt, J.; Murafa, N. Study of ground and unground leached vermiculite. *Applied Clay Science* **2009**, *44*, 178-184, doi:https://doi.org/10.1016/j.clay.2009.01.019.
20. Stawiński, W.; Węgrzyn, A.; Freitas, O.; Chmielarz, L.; Mordarski, G.; Figueiredo, S. Simultaneous removal of dyes and metal cations using an acid, acid-base and base modified vermiculite as a sustainable and recyclable adsorbent. *Science of The Total Environment* **2017**, *576*, 398-408, doi:https://doi.org/10.1016/j.scitotenv.2016.10.120.
21. Wu, W.; Cheng, C.L.; Shen, S.L.; Zhang, K.; Meng, H.; Guo, K.; Chen, J.F. Effects of silica sources on the properties of magnetic hollow silica. *Colloids and Surfaces A: Physicochemical and Engineering Aspects* **2009**, *334*, 131-136, doi:https://doi.org/10.1016/j.colsurfa.2008.10.043.
22. Kang, K.-M.; Kim, H.-W.; Shim, I.-W.; Kwak, H.-Y. Catalytic test of supported Ni catalysts with core/shell structure for dry reforming of methane. *Fuel Processing Technology* **2011**, *92*, 1236-1243, doi:https://doi.org/10.1016/j.fuproc.2011.02.007.
23. Daza, C.E.; Kiennemann, A.; Moreno, S.; Molina, R. Dry reforming of methane using Ni–Ce catalysts supported on a modified mineral clay. *Applied Catalysis A: General* **2009**, *364*, 65-74, doi:https://doi.org/10.1016/j.apcata.2009.05.029.
24. Taufiq-Yap, Y.H.; Sudarno; Rashid, U.; Zainal, Z. CeO2–SiO2 supported nickel catalysts for dry reforming of methane toward syngas production. *Applied Catalysis A: General* **2013**, *468*, 359-369, doi:https://doi.org/10.1016/j.apcata.2013.09.020.
25. Wang, F.; Xu, L.; Shi, W. Syngas production from CO2 reforming with methane over core-shell Ni@SiO2 catalysts. *Journal of CO2 Utilization* **2016**, *16*, 318-327, doi:https://doi.org/10.1016/j.jcou.2016.09.001.
26. Koo, K.Y.; Roh, H.-S.; Seo, Y.T.; Seo, D.J.; Yoon, W.L.; Park, S.B. Coke study on MgO-promoted Ni/Al2O3 catalyst in combined H2O and CO2 reforming of methane for gas to liquid (GTL) process. *Applied Catalysis A: General* **2008**, *340*, 183-190, doi:https://doi.org/10.1016/j.apcata.2008.02.009.
27. Zhao, X.; Cao, Y.; Li, H.; Zhang, J.; Shi, L.; Zhang, D. Sc promoted and aerogel confined Ni catalysts for coking-resistant dry reforming of methane. *RSC Advances* **2017**, *7*, 4735-4745, doi:10.1039/C6RA27266E.

28. Li, M.; van Veen, A.C. Coupled reforming of methane to syngas (2H2-CO) over Mg-Al oxide supported Ni catalyst. *Applied Catalysis A: General* **2018**, *550*, 176-183, doi:https://doi.org/10.1016/j.apcata.2017.11.004.
29. Damyanova, S.; Pawelec, B.; Arishtirova, K.; Fierro, J.L.G.; Sener, C.; Dogu, T. MCM-41 supported PdNi catalysts for dry reforming of methane. *Applied Catalysis B: Environmental* **2009**, *92*, 250-261, doi:https://doi.org/10.1016/j.apcatb.2009.07.032.
30. Zhang, W.D.; Liu, B.S.; Tian, Y.L. CO2 reforming of methane over Ni/Sm2O3–CaO catalyst prepared by a sol–gel technique. *Catalysis Communications* **2007**, *8*, 661-667, doi:https://doi.org/10.1016/j.catcom.2006.08.020.
31. Yoshida, H.; Yamaoka, R.; Arai, M. Stable Hydrogen Production from Ethanol through Steam Reforming Reaction over Nickel-Containing Smectite-Derived Catalyst. *International Journal of Molecular Sciences* **2015**, *16*, 350-362, doi:10.3390/ijms16010350.
32. Trevisanut, C.; Mari, M.; Millet, J.-M.M.; Cavani, F. Chemical-loop reforming of ethanol over metal ferrites: An analysis of structural features affecting reactivity. *International Journal of Hydrogen Energy* **2015**, *40*, 5264-5271, doi:https://doi.org/10.1016/j.ijhydene.2015.01.054.
33. Carrasco-Ruiz, S.; Zhang, Q.; Gándara-Loe, J.; Pastor-Pérez, L.; Odriozola, J.A.; Reina, T.R.; Bobadilla, L.F. H2-rich syngas production from biogas reforming: Overcoming coking and sintering using bimetallic Ni-based catalysts. *International Journal of Hydrogen Energy* **2023**, *48*, 27907-27917, doi:https://doi.org/10.1016/j.ijhydene.2023.03.301.
34. Yang, E.; Nam, E.; Jo, Y.; An, K. Coke resistant NiCo/CeO2 catalysts for dry reforming of methane derived from core@shell Ni@Co nanoparticles. *Applied Catalysis B: Environmental* **2023**, *339*, 123152, doi:https://doi.org/10.1016/j.apcatb.2023.123152.
35. Wang, M.; Kim, S.Y.; Jamsaz, A.; Pham-Ngoc, N.; Men, Y.; Jeong, D.H.; Shin, E.W. Effect of active sites distributions on temperature dependent–coke formation over Ni/CexZr1−xO2–Al2O3 catalysts for ethanol steam reforming: Coke precursor gasification. *Applied Surface Science* **2024**, *644*, 158746, doi:https://doi.org/10.1016/j.apsusc.2023.158746.
36. Feng, X.; Zhao, Y.; Zhao, Y.; Wang, H.; Liu, H.; Zhang, Q. A mini review on recent progress of steam reforming of ethanol. *RSC Advances* **2023**, *13*, 23991-24002, doi:10.1039/D3RA02769D.
37. Palma, V.; Ruocco, C.; Cortese, M.; Martino, M. Bioalcohol Reforming: An Overview of the Recent Advances for the Enhancement of Catalyst Stability. *Catalysts* **2020**, *10*, doi:10.3390/catal10060665.
38. Abdelkader, A.; Daly, H.; Saih, Y.; Morgan, K.; Mohamed, M.A.; Halawy, S.A.; Hardacre, C. Steam reforming of ethanol over Co3O4–Fe2O3 mixed oxides. *International Journal of Hydrogen Energy* **2013**, *38*, 8263-8275, doi:https://doi.org/10.1016/j.ijhydene.2013.04.009.
39. Braga, A.; dos Santos, J.; Bueno, J.M.C.; Damyanova, S. Hydrogen Production by Ethanol Steam Reforming. *Athens Journal of Sciences 3*, 7-16, doi:https://doi.org/10.30958/ajs.3-1-1.
40. Ob-eye, J.; Praserthdam, P.; Jongsomjit, B. Dehydrogenation of Ethanol to Acetaldehyde over Different Metals Supported on Carbon Catalysts. *Catalysts* **2019**, *9*, doi:10.3390/catal9010066.
41. Meng, H.; Zhang, J.; Yang, Y. Recent Status in Catalyst Modification Strategies for Hydrogen Production from Ethanol Steam Reforming. *ChemCatChem* **2023**, *15*, e202300733, doi:https://doi.org/10.1002/cctc.202300733.
42. Shtyka, O.; Dimitrova, Z.; Ciesielski, R.; Kedziora, A.; Mitukiewicz, G.; Leyko, J.; Maniukiewicz, W.; Czylkowska, A.; Maniecki, T. Correction to: Steam reforming of ethanol for hydrogen production: influence of catalyst composition (Ni/Al2O3, Ni/Al2O3–CeO2, Ni/Al2O3–ZnO) and process conditions. *Reaction Kinetics, Mechanisms and Catalysis* **2021**, *134*, 1089-1089, doi:10.1007/s11144-021-02095-5.